

L4acados: Learning-based models for acados, applied to Gaussian process-based predictive control

Amon Lahr^{*1}, Joshua Näf^{*1}, Kim P. Wabersich², Jonathan Frey³, Pascal Siehl²,
Andrea Carron¹, Moritz Diehl³, Melanie N. Zeilinger¹

Abstract—Incorporating learning-based models, such as Gaussian processes (GPs), into model predictive control (MPC) strategies can significantly improve control performance and online adaptation capabilities for real-world applications. Still, despite recent advances in numerical optimization and real-time GP inference, its widespread application is limited by the lack of an efficient and modular open-source implementation. This work aims at filling this gap by providing an efficient implementation of zero-order Gaussian process-based MPC in `acados`, as well as `L4acados`, a general framework for incorporating non-`CasADi` (learning-based) residual models in `acados`. By providing the required sensitivities via a user-defined Python module, `L4acados` enables the implementation of MPC controllers with learning-based residual models in `acados`, while supporting custom Jacobian approximations, as well as parallelization of sensitivity computations when preparing the quadratic subproblems. The computational efficiency of `L4acados` is benchmarked against available software using a neural network-based control example. Last, it is used demonstrate the performance of the zero-order GP-MPC method applied to two hardware examples: autonomous miniature racing, as well as motion control of a full-scale autonomous vehicle for an ISO lane change maneuver.

Code: <https://github.com/IntelligentControlSystems/L4acados>

Index Terms—Optimization and Optimal Control, Model Learning for Control, Software Tools for Robot Programming.

I. INTRODUCTION

MODEL predictive control (MPC) with Gaussian process (GP) residual models has established itself as a highly effective and safety-aware control strategy for challenging applications such as autonomous racing [1]–[3], outdoor mobile robots [4], [5] and other robotic applications [6]. Yet, to ensure real-time feedback control despite its high computational requirements, most GP-MPC implementations are tailored to their specific use case, which complicates translation to other applications. Specifically, real-time GP-MPC applications face two main challenges – complexity of the optimization problem and available software.

First, propagation of the state covariances inside the optimal control problem (OCP) introduces a large additional number of

optimization variables, which leads to an unfavorable scaling of the computational complexity with respect to the state dimension. To mitigate this, the GP posterior covariances are largely not considered inside the optimization problem [3], [4], or heuristically fixed based on the state-input trajectory obtained at the previous sampling time of the model predictive controller [1], [2], [6], [7]. This problem has been alleviated by leveraging the zero-order robust optimization (zoRO) algorithm for GP-MPC [8]. The zoRO algorithm, initially proposed in the stochastic [9] and later in the robust MPC setting [10], propagates the covariances between each iteration of the Newton-type optimization method used to solve the OCP. It has seen successful applications in obstacle avoidance problems using nonlinear robust MPC [11], as well as for friction-adaptive autonomous driving [12]. Similar optimization strategies have also been employed by [5], using a log-barrier constraint relaxation for control of an outdoor robot, and by [13], employing a linear-parameter-varying reformulation of the GP-MPC problem.

Second, while significant advancements have been made in computationally efficient (approximate) GP inference [14], enabling these for fast-sampled GP-MPC applications remains challenging due to the difficulty of interfacing machine learning frameworks such as `PyTorch`, `TensorFlow` and `JAX`, with optimal control software such as `CasADi` [15] and `acados` [16]. To this end, existing real-time GP-MPC implementations commonly resort to custom GP implementations (see, e.g., [1], [3]), lagging behind the state-of-the-art in terms of kernel design, hyper-parameter optimization, available GP approximations, and parallelization capabilities. The same applies to a large share of available software for coupling optimal control frameworks with learning-based models: `HILo-MPC` [17] supports artificial neural networks and vanilla GP regression by re-implementing them within `CasADi`. Similarly, `LbMATMPC` [18] re-implements the GP mean and its Jacobian in `CasADi` as a vector product with precomputed weights. In the `safe-control-gym` [19] implementation of the GP-MPC method by [2], GP inference is partly manually formulated with `CasADi` symbolics and partly directly evaluated in `GPpyTorch`. For neural networks, `do-mpc` [20] incorporates models adhering to the ONNX standard as `CasADi` models. A more general approach is followed by `L4CasADi` [21], enabling the integration of `PyTorch` models by compiling them into the `CasADi` computational graph. Yet, beyond the restriction to traceable

^{*}Both authors contributed equally.

¹ETH Zürich, Switzerland.

²Robert Bosch GmbH, Corporate Research, Stuttgart, Germany.

³Department of Microsystems Engineering (IMTEK) and Department of Mathematics, University of Freiburg, Freiburg, Germany.

This work was supported by the European Union’s Horizon 2020 research and innovation programme, Marie Skłodowska-Curie grant agreement No. 953348, ELO-X, and by DFG via 424107692 and 504452366 (SPP 2364).

PyTorch models, L4CasADi's batch processing capabilities are not compatible with the available options for parallelized sensitivity computation in acados, complicating the efficient integration of both tools.

Contribution

In this work, we present L4acados, an open-source framework for coupling acados with general (learning-based) discrete-time residual models. Building upon the implementation in [8], L4acados directly supplies the sensitivities needed at every iteration of the sequential quadratic programming (SQP) algorithm using the acados Python interface. The framework supports general Python-callable residual models, custom Jacobian approximations, as well as parallelization of the model and Jacobian evaluation during the SQP preparation phase. In addition, we extend the recently developed, efficient implementation of the zoRO algorithm [22] inside the real-time optimization framework acados [16], to the zero-order GP-MPC (zoGPMPC) setting [8]. Utilizing L4acados in combination with GPyTorch [14], the zoGPMPC algorithm [8] is applied on the automotive miniature racing platform CRS [23], and a full-scale automotive motion controller for an ISO lane change maneuver.

II. ALGORITHM: ZERO-ORDER GP-MPC

We consider the real-time solution of MPC problems based on the discrete-time dynamics

$$x(k+1) = f(x(k), u(k)) + B_d g(x(k), u(k)) + w(k), \quad (1)$$

where $x(k) \in \mathbb{R}^{n_x}$ denotes the state of the system and $u(k) \in \mathbb{R}^{n_u}$, the control input. The system dynamics are composed of a nominal model $f: \mathbb{R}^{n_x \times n_u} \rightarrow \mathbb{R}^{n_x}$; a residual model $g: \mathbb{R}^{n_x \times n_u} \rightarrow \mathbb{R}^{n_g}$, $n_g \leq n_x$, mapped onto the full state using the matrix $B_d \in \mathbb{R}^{n_x \times n_g}$; and i.i.d. process noise $w(k) \sim \mathcal{N}(0, \Sigma_w)$, with positive semi-definite $\Sigma_w \in \mathbb{R}^{n_x \times n_x}$. The nominal model is commonly obtained by numerically integrating a continuous-time model based on first principles, while the residual model is obtained directly in discrete-time by training a Gaussian process

$$g(x(k), u(k)) \sim \mathcal{N}(\mu^d(x(k), u(k)), \Sigma^d(x(k), u(k)))$$

using subsequent state measurements,

$$y(k) \doteq B_d^\dagger (x(k+1) - f(x(k), u(k))) \quad (2)$$

$$= g(x(k), u(k)) + v(k). \quad (3)$$

The measurements $y(k)$ and corresponding noise distribution $v(k) \sim \mathcal{N}(0, B_d^\dagger \Sigma_w B_d)$ are obtained by projecting the full state onto the subspace of the residual model using the Moore-Penrose pseudo-inverse $(\cdot)^\dagger$ of B_d – a common setup for GP-MPC as done, e.g., by [2].

A. Linearization-based GP-MPC

Using a linearization-based approximation of the stochastic dynamics in terms of its mean μ_k^x and covariance Σ_k , we are

interested in solving the following approximate reformulation of the GP-MPC optimization problem [2],

$$\min_{\substack{u_0, \dots, u_{N-1} \\ \mu_0^x, \dots, \mu_N^x, \\ \Sigma_0^x, \dots, \Sigma_N^x}} \sum_{k=0}^{N-1} l(\mu_k^x, u_k) + M(\mu_N^x) \quad (4a)$$

$$\text{s.t.} \quad \mu_0^x = \bar{x}_0, \quad (4b)$$

$$\Sigma_0^x = 0, \quad (4c)$$

$$\mu_{k+1}^x = f(\mu_k^x, u_k) + B_d \mu^d(\mu_k^x, u_k), \quad (4d)$$

$$\Sigma_{k+1}^x = \Psi_k(\mu_k^x, u_k, \Sigma_k^x), \quad (4e)$$

$$0 \geq h(\mu_k^x, u_k) + \beta(\mu_k^x, u_k, \Sigma_k^x), \quad (4f)$$

$$0 \geq h_N(\mu_N^x) + \beta_N(\mu_N^x, \Sigma_N^x). \quad (4g)$$

Thereby, the discrete-time covariance dynamics are given as

$$\Psi_k(\mu_k^x, u_k, \Sigma_k^x) = A_k \Sigma_k^x A_k^\top + B_d \Sigma^d(\mu_k^x, u_k) B_d^\top + \Sigma_w, \quad (5)$$

where $A(\mu_k^x, u_k) \doteq \frac{\partial}{\partial x}(f(x, u_k) + B_d \mu^d(x, u_k))|_{x=\mu_k^x}$ denotes the Jacobian of the nominal and GP mean dynamics with respect to the (mean) state. Component-wise for each $j = 1, \dots, n_h$, the nominal constraints h_j are tightened by

$$\beta_j(\mu_k^x, u_k, \Sigma_k) \doteq \gamma_j \sqrt{C_j(\mu_k^x, u_k) \Sigma_k C_j^\top(\mu_k^x, u_k)}, \quad (6)$$

where $C_j(\mu_k^x, u_k) = \frac{\partial h_j}{\partial x}(x, u_k)|_{x=\mu_k^x}$. Assuming a Gaussian state density, $p_j = \Phi(\gamma_j)$ thereby corresponds to the approximate satisfaction probability of the linearized one-sided constraint, with $\Phi(\cdot)$ denoting the cumulative density function of a standard normal Gaussian variable.

B. Zero-order algorithm

Despite the approximations, the solution of the GP-MPC OCP (4) still remains intractable for many real-time applications due to increased number of states and computationally expensive evaluations of the GP, in particular the gradients of the posterior covariance, as well as the Hessian of the posterior mean. Following the procedure in [8], we thus employ the zoRO method [9], [10] to obtain a suboptimal, yet feasible, point of the OCP at drastically reduced computation cost. Starting with an initial guess for the input and mean variables \hat{u}_k and $\hat{\mu}_k^x$, respectively, the zoRO algorithm performs sequential quadratic programming (SQP) iterations with a tailored Jacobian approximation, alternating the covariance propagation (4e), for all $k = 0, \dots, N-1$, with the solution of the reduced-size, quadratic subproblem

$$\min_{\Delta \mu^x, \Delta u} \sum_{k=0}^{N-1} \begin{bmatrix} \Delta \mu_k^x \\ \Delta u_k \\ 1 \end{bmatrix}^\top \begin{bmatrix} Q_k & S_k & q_k \\ & R_k & r_k \\ \star & & 1 \end{bmatrix} \begin{bmatrix} \Delta \mu_k^x \\ \Delta u_k \\ 1 \end{bmatrix} \quad (7a)$$

$$\text{s.t.} \quad \Delta \mu_0^x = 0 \quad (7b)$$

$$\Delta \mu_{k+1}^x = f(\hat{\mu}_k^x, \hat{u}_k) + B_d g(\hat{\mu}_k^x, \hat{u}_k) - \hat{\mu}_{k+1}^x + \hat{A}_k \Delta \mu_k^x + \hat{B}_k \Delta u_k, \quad (7c)$$

$$0 \geq h(\hat{\mu}_k^x, \hat{u}_k) + \hat{H}_k^x \Delta \mu_k^x + \hat{H}_k^u \Delta u_k + \tilde{\beta}_k, \quad (7d)$$

$$0 \geq h(\hat{\mu}_N^x) + \hat{H}_N^x \Delta \mu_N^x + \tilde{\beta}_N. \quad (7e)$$

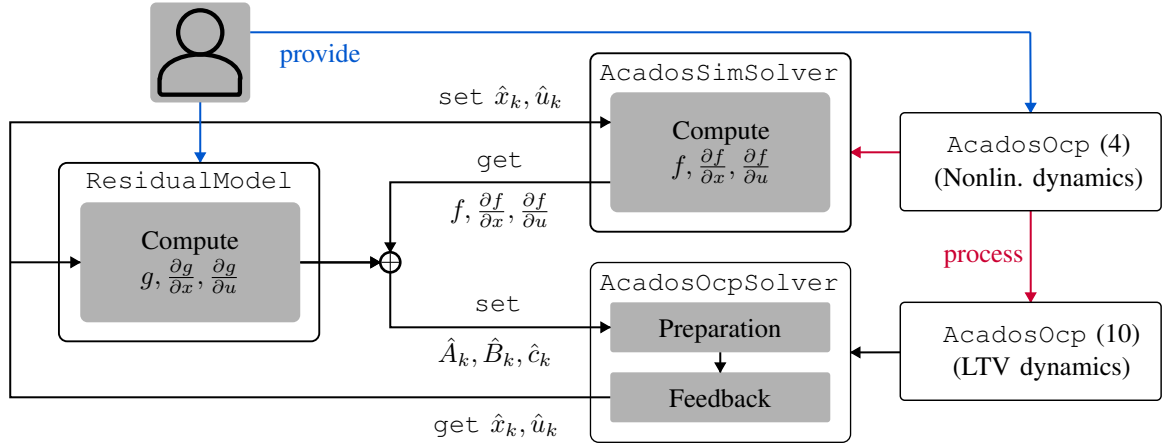


Fig. 1: Flow diagram of SQP iterations in L4acados. By using the `acados` Python interface to `get/set` the model sensitivities in each SQP iteration, L4acados enables learning-based models for real-time optimal control with `acados`.

Thereby, Q_k, R_k, S_k define the employed Hessian approximation and q_k, r_k , the linear penalty term. The nonlinear equality and inequality constraints are linearized, with Jacobians

$$\hat{A}_k = \left. \frac{\partial(f + B_d g)}{\partial x} \right|_{\substack{x=\hat{\mu}_k^x \\ u=\hat{u}_k}}, \quad \hat{B}_k = \left. \frac{\partial(f + B_d g)}{\partial u} \right|_{\substack{x=\hat{\mu}_k^x \\ u=\hat{u}_k}}, \quad (8)$$

$$\hat{H}_k^{\{x,u\}} = \left. \frac{\partial h}{\partial \{x,u\}} \right|_{\substack{x=\hat{\mu}_k^x \\ u=\hat{u}_k}}, \quad \hat{H}_N = \left. \frac{\partial h_N}{\partial x} \right|_{x=\hat{\mu}_k^x}. \quad (9)$$

Note that the presented version of the zoRO algorithm employs an additional Jacobian approximation compared to the one in [8] by neglecting the Jacobians of the back-off term $\beta(x, u, \Sigma)$, as it has also been done in [11], [22].

III. SOFTWARE: L4ACADOS

To enable efficient treatment of learning-based models in `acados`, L4acados requires two user inputs (see Fig. 1): an `AcadosOcp` defining the OCP formulation for the nominal model f , and a `ResidualModel` for the external residual model g . L4acados modifies the OCP, such that the corresponding `AcadosOcpSolver` allows one to externally specify the residual model's contributions at each SQP iteration. This way, L4acados avoids cumbersome re-implementations of existing models in `CasADi`, reduces maintenance requirements, and integrates into the open-source ecosystem.

A. `acados` OCP formulation

In order to use non-`CasADi` tools to evaluate and differentiate the residual model, L4acados converts the nonlinear OCP (4) into an OCP with affine dynamics, i.e.,

$$\min_{\substack{u_0, \dots, u_{N-1} \\ \mu_0^x, \dots, \mu_N^x}} \sum_{k=0}^{N-1} l(\mu_k^x, u_k) + M(\mu_N^x) \quad (10a)$$

$$\text{s.t.} \quad \mu_0^x = \bar{x}_0 \quad (10b)$$

$$\mu_{k+1}^x = \hat{A}_k \mu_k^x + \hat{B}_k u_k + \hat{c}_k, \quad (10c)$$

$$0 \geq h(\mu_k^x, u_k) + \tilde{\beta}_k, \quad (10d)$$

$$0 \geq h_N(\mu_N^x) + \tilde{\beta}_N, \quad (10e)$$

where \hat{A}_k, \hat{B}_k and \hat{c}_k are treated as model parameters. Setting

$$\hat{c}_k \doteq f(\hat{\mu}_k^x, \hat{u}_k) + B_d g(\hat{\mu}_k^x, \hat{u}_k) - \hat{A}_k \hat{\mu}_k^x - \hat{B}_k \hat{u}_k \quad (11)$$

and \hat{A}_k, \hat{B}_k at each SQP iteration according to (8) recovers the original dynamics linearization (7c) exactly. This way, L4acados recovers the same SQP iterates as obtained by solving (7) under the same Hessian approximation in Eq. (7a). This is the case for Hessian approximations that do not depend on second-order information of the dynamics, such as the generalized Gauss-Newton approximation.

Automatic conversion of the nonlinear OCP is performed by replacing the original model with the linearized discrete-time dynamics (10c). Thereby, the nominal dynamics are extracted as an `AcadosSimSolver` object, which efficiently integrates the dynamics and computes the sensitivities [24]

$$f(\hat{\mu}_k^x, \hat{u}_k), \quad \frac{\partial f}{\partial x}(\hat{\mu}_k^x, \hat{u}_k), \quad \frac{\partial f}{\partial u}(\hat{\mu}_k^x, \hat{u}_k). \quad (12)$$

In a similar fashion, it is also possible to incorporate external sensitivity information into the cost and constraints of the OCP.

B. Residual model

In L4acados, the residual model's value and Jacobians

$$g(\hat{\mu}_k^x, \hat{u}_k), \quad \frac{\partial g}{\partial x}(\hat{\mu}_k^x, \hat{u}_k), \quad \frac{\partial g}{\partial u}(\hat{\mu}_k^x, \hat{u}_k) \quad (13)$$

at the linearization points are supplied by a user-defined residual model. This retains flexibility, as any Python-callable programs can be used for providing the quantities in (13).

To enable parallelization of the sensitivity computation across the prediction horizon, the `ResidualModel` is called *once* using a batch of the linearization points (\hat{X}, \hat{U}) , where $\hat{X} = [\hat{\mu}_0^x, \dots, \hat{\mu}_{N-1}^x]$, $\hat{U} = [\hat{u}_0, \dots, \hat{u}_{N-1}]$ are the concatenated states and inputs, respectively, at the current iterate. In particular for computationally expensive residual models, parallelization of the residual model (sensitivity) evaluation can lead to significant speed-ups, offsetting overheads incurred when transferring data between different devices for optimization and residual model evaluation, see Section III-E.

C. Real-time iteration with *L4acados*

A popular strategy to reduce latency of the optimization-based controller is the Real-Time Iteration (RTI) [25], which executes a single SQP iteration per sampling time, split into two phases: During the preparation phase the sensitivity computations are performed, while the next initial state \bar{x}_0 is not yet available. After it has been received, during the feedback phase, the prepared QP is solved and the first input is applied to the real system. Using the same splitting, the approach taken in *L4acados* can be seen as performing (parts of) the sensitivity computations during the RTI preparation phase outside of *acados*. During *acados*' internal preparation phase (see Fig. 1), the remaining computations for setting up the quadratic subproblem are executed.

D. Possible applications of *L4acados*

Since the numerical values of $\hat{A}_k, \hat{B}_k, \hat{c}_k$ are directly passed as model parameters, *L4acados* enables a variety of possible use cases: 1) Learning-based models implemented in machine learning frameworks such as `PyTorch`, `TensorFlow` and `JAX`; 2) Black-box models without gradient information (by returning no Jacobian or a finite-difference approximation); 3) Custom Jacobian approximations, e.g., multi-level iterations [26], feasible SQP [27], with learning-based models; 4) Online model updates in `Python`. In the following sections, we demonstrate the use of *L4acados* with `PyTorch` models and online updates using a `GPYtorch` GP implementation.

E. *L4CasADi* vs. *L4acados*

In this section, the computational efficiency and scaling of *L4acados* is compared against *L4CasADi* for a double-integrator system with added neural-network (NN) dynamics¹, where all weights of the NN have been set to zero, i.e., $g(x(k)) = \text{NN}(x(k)) \equiv 0$. As similarly done in [28], this allows one to scale the number of layers $\#_{\text{layers}}$ of the multi-layer perceptron without affecting the MPC solution; the number of neurons per layer is set to 512.

In Fig. 2, the computation time and scaling of both methods (top row), as well as the achieved speedup of *L4acados* (bottom row), is evaluated for an increasing prediction horizon N , NN complexity (indicated by the number of layers $\#_{\text{layers}}$ of the `PyTorch` multi-layer perceptron), and parallelization configurations ‘‘DEV-TX-AY’’. Here, $\text{DEV} \in \{\text{CPU}, \text{GPU}\}$ indicates whether the NN is evaluated on the CPU or GPU (with CUDA), respectively; X , the number of respective CPU cores in case of CPU parallelization; and Y , the number of CPU cores used for parallelizing the sensitivity evaluation in *acados* with OpenMP, where $Y = 0$ denotes that *acados* is compiled without OpenMP parallelization.

Across all parallelization configurations considered, *L4acados* achieves already noticeable speedups for typically-short prediction horizons $N \geq 10$, which become more pronounced as the model complexity is increased. Parallelization of the NN evaluations on the CPU (‘‘CPU-T10’’) or GPU (‘‘GPU-T1-’’) thereby leads to slight speedups

for $\#_{\text{layers}} = 20$ layers for both approaches; for fewer layers, to slightly larger computation times. Most prominent is the different scaling for varying lengths of the prediction horizon: For *L4CasADi*, the linear scaling of the computation time for all ‘‘-A0’’ scenarios is due to the sequential sensitivity computation in *acados*. The last column shows that using *acados*' built-in OpenMP parallelization of sensitivity computations in conjunction with *L4CasADi* affects its scaling properties; however, it does not lead to computational benefits². In contrast, by computing sensitivities in parallel outside *acados*, *L4acados* shows an improved scaling throughout all scenarios, approaching the linear scaling as the ratio between available cores and horizon length decreases. Parallelization of the sensitivity evaluations for the ‘‘CPU-T1-A10’’ scenario has a negligible effect on the *L4acados* timings, as the sensitivity computations within *acados*, corresponding to the linearized dynamics, are trivial.

IV. ZERO-ORDER GP-MPC USING *L4ACADOS*

In this section, *L4acados* is used for an efficient implementation of GP-MPC (Section IV-A), and applied both in simulation and hardware for real-time control on two autonomous driving platforms (see Fig. 3): miniature racing using CRS [23] (Section IV-B) and motion control of a full-scale vehicle for an ISO lane change maneuver (Section IV-C).

A. Zero-order GP-MPC implementation using *L4acados*

Using *L4acados*, the zero-order GP-MPC method [8] is implemented by defining a `GPYtorch` [14] residual model for efficient and parallelizable GP computations, as well as extending the zoRO custom update function [22] in *acados* for efficient uncertainty propagation with BLASFEO [29].

1) *GPYtorch ResidualModel*: While the main function of the `ResidualModel` is to provide evaluations and sensitivities of the GP posterior mean, for the zoGPMPC implementation it has been extended to i) compute and store the GP posterior covariance; ii) GP input feature selection; iii) adding of various data processing strategies, facilitating the recording of data points as well as GP model updates.

2) *acados custom update function*: In between SQP iterations, the zoGPMPC algorithm propagates the state covariances according to (5). To this end, the efficient zoRO implementation presented in [22], which utilizes the high-performance linear algebra package BLASFEO [29], has been extended to support a time-varying process noise component, which is used to incorporate evaluations of the GP posterior covariance in the covariance prediction.

B. Autonomous miniature racing

The proposed implementation is tested on the CRS robotics software platform [23], which is used for autonomous racing

²The same can be observed when admitting only a single core for `PyTorch` parallelization, i.e., in the configuration ‘‘CPU-T1-A10’’, which is not shown due to space limitations. Using both *L4CasADi* and *acados* with OpenMP parallelization, i.e., ‘‘CPU-T10-A10’’, led to considerably slower computation times, as well as leaked memory at every solver call.

¹Code: <https://github.com/IntelligentControlSystems/L4acados>

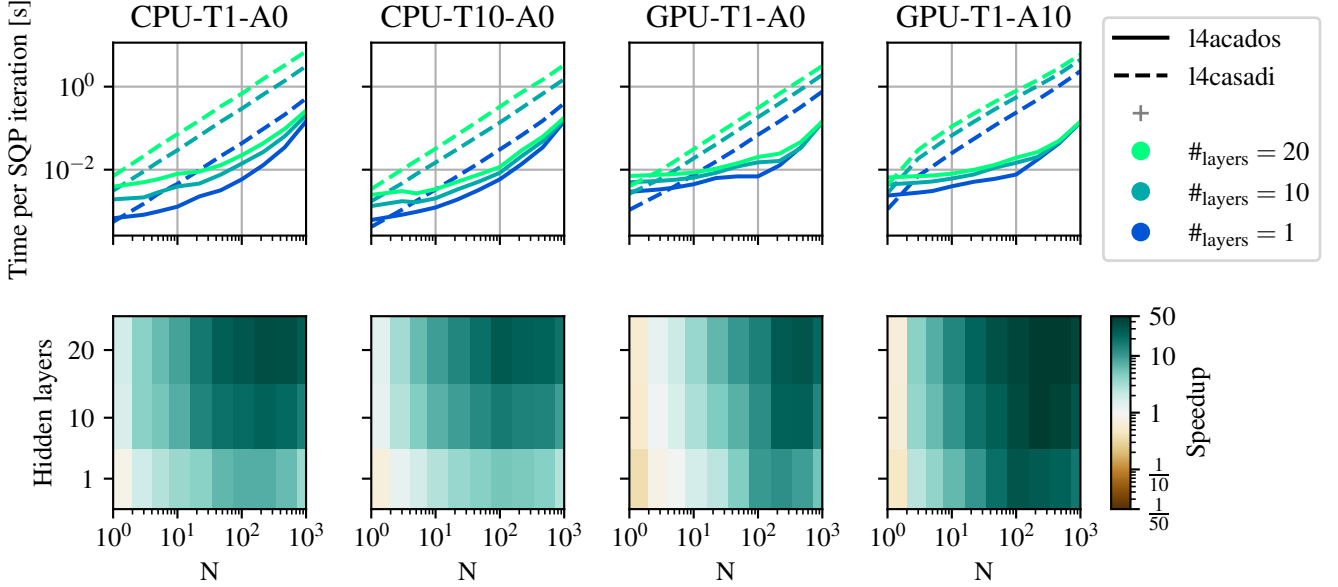


Fig. 2: Comparison of solve times for a neural-network residual model (Section III-E). Already for small horizon lengths and moderate learning-based-model complexities, L4acados shows drastic speedups compared to using acados with L4CasADi.

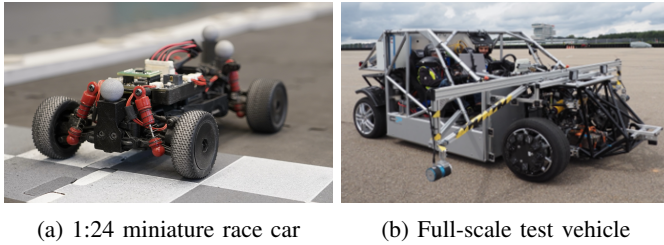


Fig. 3: Hardware platforms.

in simulation³ as well as on hardware⁴, using a custom 1:24 miniature R/C car based on a Mini-Z MB010 four-wheel drive chassis (see Fig. 3a) and a Qualisys motion capture system.

The controller is formulated akin to the model predictive contouring control (MPCC) formulation of [30, Eq. (13)], where the state $\mu_k^x = (x, y, \psi, v_x, v_y, \omega, T, \delta, \theta) \in \mathbb{R}^9$ contains the mean x -, y -position and heading angle ψ in a global coordinate frame, lateral and longitudinal velocities v_x and v_y , as well as yaw rate ω in a local coordinate frame, respectively. Additionally, the states T and δ denote the applied torque and steering angle, respectively, and θ , the progress of the car along the track. The nominal model is then composed of the combined dynamics of the kinematic bicycle model using a simplified Pacejka tire model (see, e.g., [23, Sec. V.A.2]), and simple integrators for the torque and steering angle’s actuator dynamics, as well as for the progress variable. For the latter, the corresponding velocities are the control inputs $u_k \doteq (\dot{T}, \dot{\delta}, \dot{\theta}) \in \mathbb{R}^3$. The MPCC problem can then be expressed as problem (4) with zero terminal cost, $M(\mu_N^x) = 0$, and a nonlinear-least-squares

stage cost $l(\mu_k^x, u_k) = \|y(\mu_k^x, u_k)\|_{Q^y}^2$, where the regressor $y(\mu_k^x, u_k) = (e^c(x_k, y_k, \theta_k), e^l(x_k, y_k, \theta_k), \dot{T}_k, \dot{\delta}_k, \dot{\theta}_k, 1)$ contains the contouring and lag error terms e^c and e^l , respectively, as well as the inputs $\dot{T}_k, \dot{\delta}_k, \dot{\theta}_k$. Using the additional constant term, the MPCC cost can be expressed by appropriately defining the positive definite penalty matrix Q^y .

As the most severe modeling errors are considered to be in the Pacejka tire friction model and corresponding parameter estimates, a GP is used to learn the residual of the discrete-time velocity predictions, i.e., $B_d^T \doteq [0_{3 \times 3} \quad I_{3 \times 3} \quad 0_{3 \times 3}]$. To reduce the dimensionality of the input space, and the associated risk of overfitting to irrelevant features, the GP input features are chosen as $(v_x, v_y, \omega, T, \delta)$.

1) *Simulation results:* To evaluate computation times in a more controlled environment for different solver configurations, runtime experiments are performed in a ROS simulation for a fixed number of $N_{\text{sim}} = 3000$ simulation steps at a sampling frequency of 30Hz, amounting to a 100s time limit. The “ground-truth” car dynamics is thereby given by the set of Pacejka friction parameters obtained from system identification, while the nominal car dynamics use values that have been slightly perturbed; in particular, the perturbed model assumes rear-wheel drive instead of four-wheel drive and overestimates the grip, leading to unsafe driving behavior.

Fig. 4 shows the closed-loop constraint evaluation of the track constraint for SQP-RTI controllers using different models. Separated by the dashed lines, the green zone denotes the (soft) constraint implemented in the controller; the yellow zone, an additional safety margin to the track boundary; the red zone, the track limits. In the top plot, it can be seen that the controller based on the exact model operates close to the track constraint. While for the exact model the car stays within the defined safety margins at all times, for the

³Code: <https://gitlab.ethz.ch/ics/crs>

⁴Experiment data and videos: doi:10.3929/ethz-b-000707631

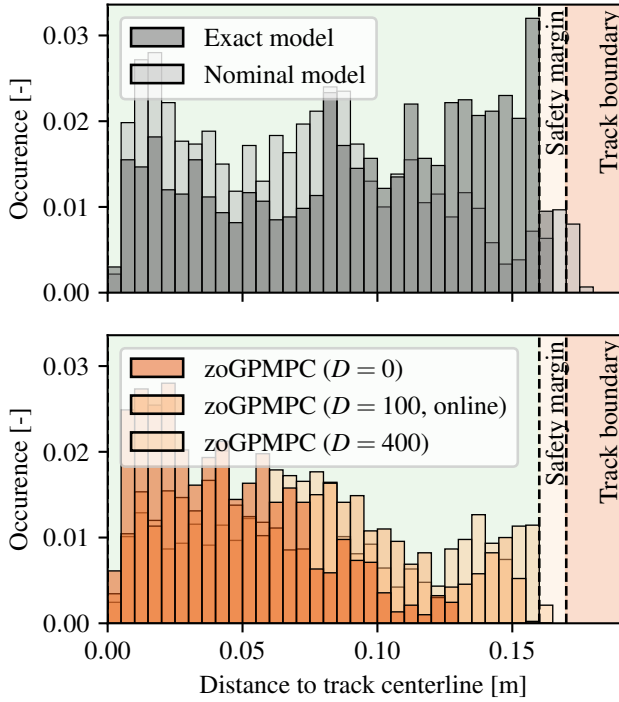


Fig. 4: Distance between miniature race car and centerline in closed-loop simulations. Augmented with real-world data, the uncertainty-aware GP model reduces conservatism to cautiously improve driving performance.

nominal model track constraint violations (i.e. crashes) occur. The small proportion of (soft) constraint violations using the exact model can be attributed to approximate convergence within the real-time iterations, as well as delays in the ROS simulator. In the lower plot, the constraint evaluations for the zoGPMPC method are shown. For $D = 0$ data points, i.e., the prior GP uncertainty, the car stays close to the centerline; for $D \in \{100, 400\}$ points, much more aggressive driving behavior is observed. Notably, in all cases, the track constraints are respected, showcasing the potential for high-performance, yet uncertainty-aware, learning-based control.

In Table I, a variety of solver configurations is compared:

Covariance updates: *zero-order* updates denote recomputed constraint tightenings at each SQP iteration, in contrast to *fixed* covariances based on the predicted trajectory at the previous sampling time⁵; both variants are equivalent for *SQP-RTI*.

Optimizer: *SQP* is used to solve the OCP iteratively at each sampling time until convergence while *SQP-RTI* performs a single iteration at each sampling time. For the simulations, an iterate with all KKT residuals smaller than $\text{tol} \doteq 10^{-4}$ is considered converged; the maximum number of SQP iterations is set to 30. To meet sampling time requirements for all methods, the simulation time is scaled by $\alpha_{\text{RTI}} \doteq 0.5$ for *SQP-RTI* scenarios and by $\alpha_{\text{SQP}} \doteq 0.015$ for *SQP* scenarios.

GP model: All GP models are implemented using GPyTorch [14]. The *exact* GP model obtains the posterior mean and covariance using an (offline) Cholesky decomposition of the kernel matrix; the *inducing-point* GP model, using the subset-of-regressors approximation [31, Sec. 8.3.1] with 10

inducing points, re-distributed along the previously predicted input-feature trajectories at each sampling time; the *online* implementation, an exact GP model incorporating new data points at every sampling time, randomly replacing old data points once a pre-specified limit is reached, with recursive up- and down-dates of the kernel matrix’ Cholesky factors (see, e.g., [32, Appendix B]).

Time: Total computation times (*total*) are split into preparation (*prep.*) and feedback (*fbk.*), the former including all computations that can be performed before sampling the next initial state, the latter, the remaining computations.

Cost: This column shows the average stage cost for the closed-loop trajectory i.e., $\frac{1}{N_{\text{sim}}} \sum_{k=1}^{N_{\text{sim}}} l(x(k), u(k))$.

Laps: The progress made within the N_{sim} simulation steps, in terms of the number of laps completed, is shown here.

Crash: To compensate for delays, approximate convergence and unmodeled real-world effects, the (soft) track constraint is tightened by an additional safety margin (see Fig. 4). An “ \mathbf{X} ” indicates violation of the original track constraint.

Comparing the optimizer, it can be seen that throughout all experiments, *SQP* performs slightly better than its *SQP-RTI* counterpart in terms of closed-loop cost and track progress, at the expense of considerably increased computation times due to the higher number of SQP iterations. Regarding the GP model, the inducing-point approximation performs similarly well as the exact GP model; however, perhaps surprisingly, at a higher computational cost. This may be attributed to the fact that the exact GP model allows one to reuse the precomputed Cholesky factor, while re-distributing inducing points at each sampling time requires one to refactorize the approximated covariance matrix. The online-updating version of the exact model is real-time feasible up to roughly 100 data points.

2) *Hardware experiments:* The racing experiment has been repeated on hardware using the three *SQP-RTI* variants of zoGPMPC in Table I with an exact GP model; Fig. 5 shows the corresponding closed-loop trajectories and car velocities. As expected, the “unconditioned” variant with $D = 0$ data points in Fig. 5a) keeps the car closer to the centerline⁶. Fig. 5b) shows the zoGPMPC method with $D = 400$ random data points recorded in the previous “unconditioned” experiment: The car drives significantly more aggressively, at higher speeds and taking sharper corners. A similar driving performance is achieved using the online learning strategy with $D = 100$ data points; the transition from a more cautious to a more aggressive racing line is apparent in Fig. 5c) and d), which depict the first and sixth lap of the same experiment, respectively.

⁴Entries are rounded to the first significant digit. “ $a \pm b$ ” indicates “mean computation time a with standard deviation b ”, in milliseconds.

⁵While not exactly corresponding to the original implementation, which employed a commercial interior-point solver, this variant uses fixed covariances based on the last sampling time during optimization while solving the OCP (with correspondingly fixed tightenings) to convergence, as done in [2].

⁶Noteworthy, due to the neglected Jacobians of the covariances with respect to the states and inputs in the optimizer, the *zero-order* method, and the *fixed* variant, do not take the effect of the inputs on the size of the covariances; the reduction of the car velocity follows solely from the tighter track constraint, forcing the car to stay on the centerline.

TABLE I: Performance comparison of different GP-MPC variants in simulation for autonomous miniature racing.

Name	Covariance	Optimizer	GP Model	D	Time, total ⁴	Time, prep ⁴	Time, fdbk ⁴	Cost ⁴	Laps ⁴	Crashed
Exact model	-	SQP-RTI	-	-	5.9 ± 1.1	3.3 ± 0.6	2.6 ± 0.6	3.4	20.3	
Nominal model	-	SQP-RTI	-	-	6.0 ± 0.6	3.3 ± 0.3	2.6 ± 0.3	3.5	20.4	✗
zoGPMPC	zero-order	SQP-RTI	exact	0	6.6 ± 0.5	4.2 ± 0.3	2.4 ± 0.3	4.3	15.7	
zoGPMPC	zero-order	SQP-RTI	exact	400	11.9 ± 0.9	9.5 ± 0.7	2.4 ± 0.3	3.6	19.4	
zoGPMPC	zero-order	SQP-RTI	inducing	400	35.5 ± 1.7	33.1 ± 1.6	2.4 ± 0.3	3.6	19.4	
zoGPMPC	zero-order	SQP-RTI	exact/online	100	16.5 ± 2.0	14.1 ± 1.9	2.5 ± 0.3	3.9	17.2	
Exact model	-	SQP	-	-	91.7 ± 36.5	2.6 ± 0.3	89.0 ± 36.5	3.4	20.8	
Nominal model	-	SQP	-	-	96.8 ± 40.1	2.6 ± 0.2	94.2 ± 40.1	3.5	21.1	✗
zoGPMPC	zero-order	SQP	exact	0	121.2 ± 38.6	3.5 ± 0.3	117.7 ± 38.5	4.2	16.4	
zoGPMPC	zero-order	SQP	exact	400	238.9 ± 92.9	8.6 ± 0.5	230.3 ± 92.9	3.5	20.1	
Cautious GPMPC ⁵	fixed	SQP	exact	400	173.8 ± 67.8	8.5 ± 0.9	165.3 ± 67.7	3.5	20.2	

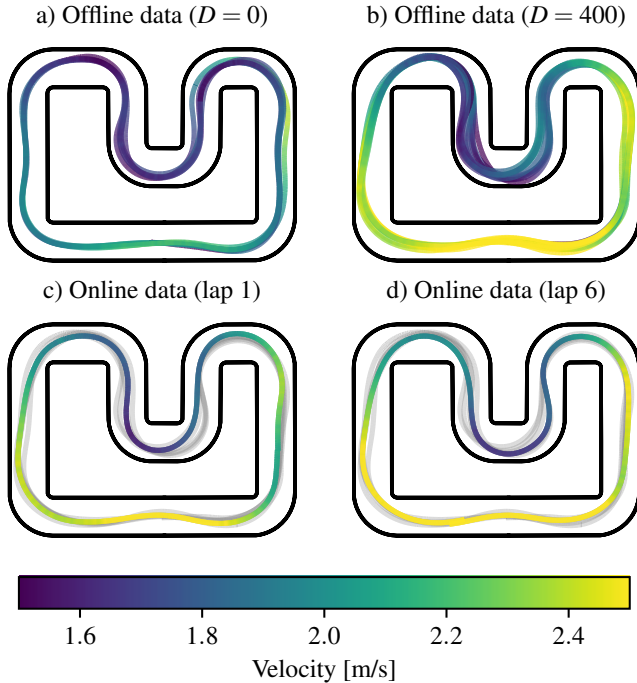


Fig. 5: Closed-loop performance comparison in miniature-racing hardware experiments (Section IV-B). In the offline and online learning setting, augmenting the nominal model with a GP leads to improved driving performance.

C. Motion control of full-scale vehicle

To demonstrate its applicability, `L4acados` is used for safe learning-based control of a research vehicle (Fig. 3b). The controller is formulated similarly to the autonomous-racing case in Section IV-B, using a slightly modified system model with states $\mu_k^x = (x, y, \psi, v, \beta, \omega, \delta, \delta_{\text{des}}, a_x, \theta) \in \mathbb{R}^{10}$ and inputs $u_k \doteq (a_x, \delta, \theta) \in \mathbb{R}^3$. Here, the slip angle β and the effective velocity v are a different representation of v_x, v_y in Section IV-B. The additional states δ_{des} and δ represent a first-order lag element to capture the steer-by-wire dynamics; a_x , the desired acceleration interface provided by the vehicle platform. The model is discretized for $N = 20$ steps using 4th-order Runge-Kutta integrator with step size 0.1 [s]. The motion control task is to comfortably track a given path with a reference velocity v_{ref} , yielding the mod-

ified regressor $y(\mu_k^x, u_k) = (e_k^c, e_k^l, v_k, \omega_k, \dot{a}_k, \dot{\delta}_{\text{des},k}, \dot{\theta}_k, v_{\text{ref}})$, subject to the safety-critical constraint of staying within the track boundaries and box constraints $\beta \in [-0.17, 0.17]$ [rad], $v \in [0.5, 40]$ [m/s], $\delta, \delta_{\text{des}} \in [0.61, 0.61]$ [rad], $\dot{\delta}_{\text{des}} \in [-0.35, 0.35]$ [rad/s], $a_x \in [-5, 5]$ [m/s²], $\dot{a}_x \in [-4, 4]$ [m/s³]. The GP is used to correct velocity predictions and the steering dynamics, i.e., $B_d \doteq [0_{3 \times 4} \quad I_{4 \times 4} \quad 0_{3 \times 4}]$, with GP inputs $(v, \beta, \omega, \delta, \delta_{\text{des}}, a_x)$.

We show the effect of including the GP model via `L4acados` using a double lane change maneuver based on the ISO 3888-1 standard (without an increasing corridor) at 30 km/h, see Fig. 6. First, a basic nominal model parameterization is applied, with *SQP-RTI*. The control performance is unsatisfactory in terms of actuator load, comfort, and stable tracking of the desired path. Equally spaced data points ($D = 136$) along the driven path are used to fit an exact GP model as described in Section IV-B using basic data preprocessing. The experiment was repeated with the same nominal model extended by the GP correction term, with a desired probability level of $p_x \doteq 95\%$ for satisfying the safety-critical path constraint. The result shows significant improvements in all performance aspects: Reduced actuation requests lead to a more comfortable driving experience, and accurate tracking of the desired path provides stable behavior. Furthermore, while the predicted confidence estimate is mostly contained within the path constraints, larger uncertainties at the end of the planning horizon act similar to a small terminal set constraint, further stabilizing the performance. The computations performed on an HP Zbook 16 Fury G10 notebook resulted in total computation times of 3.1 ± 1.4 ms and 8.2 ± 1.4 ms for the nominal MPC and zoGPMPC method, respectively – well within the control cycle time of 20ms.

V. CONCLUSIONS AND OUTLOOK

The proposed software `L4acados` enables efficient and parallelizable sensitivity computations for learning-based Python models in `acados`. Applied to GP-MPC, the presented hardware experiments for autonomous miniature racing and a full-scale autonomous vehicle prototype demonstrate the efficiency and applicability of the software. For future work, extensions to learning-based constraint and cost modules, as well as full integration of external, batched sensitivity computations in `acados` can further increase its range of potential applications and ease of use.

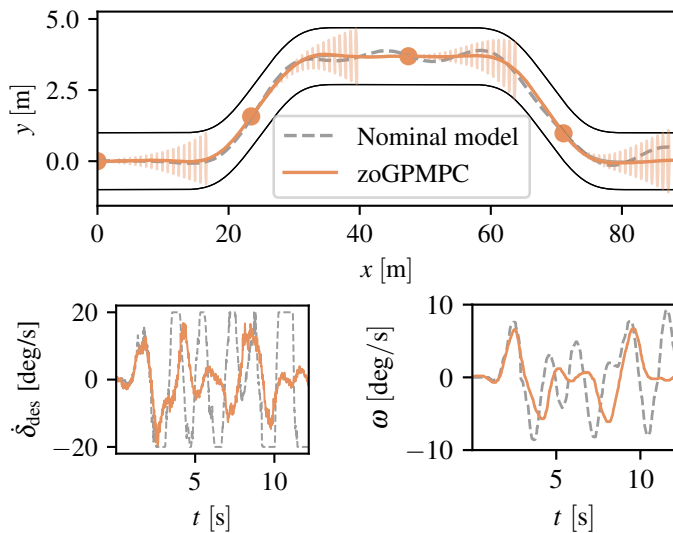


Fig. 6: Double lane change maneuver of the full-scale vehicle (Figure 3b) at 30 km/h. The nominal MPC controller yields unsatisfactory performance; the zoGPMPC method provides significant improvements. The bars indicate 95% confidence intervals that are used to tighten the track boundary constraints.

ACKNOWLEDGMENT

The authors would like to thank Tim Salzmann for a clarifying discussion regarding the benefits and limitations of L4acados compared to L4CasADi, as well as Lars Bartels and Alexander Hansson for their contributions to L4acados.

REFERENCES

- [1] J. Kabzan, L. Hewing, A. Liniger, and M. N. Zeilinger, "Learning-Based Model Predictive Control for Autonomous Racing," *IEEE Robot. Autom. Lett.*, vol. 4, no. 4, 2019.
- [2] L. Hewing, J. Kabzan, and M. N. Zeilinger, "Cautious Model Predictive Control Using Gaussian Process Regression," *IEEE Trans Control Syst Technol*, vol. 28, no. 6, 2020.
- [3] G. Torrente, E. Kaufmann, P. Föhn, and D. Scaramuzza, "Data-Driven MPC for Quadrotors," *IEEE Robotics and Automation Letters*, vol. 6, no. 2, 2021.
- [4] C. J. Ostafew, A. P. Schoellig, and T. D. Barfoot, "Learning-based nonlinear model predictive control to improve vision-based mobile robot path-tracking in challenging outdoor environments," in *2014 IEEE International Conference on Robotics and Automation (ICRA)*, 2014.
- [5] —, "Robust Constrained Learning-based NMPC enabling reliable mobile robot path tracking," *The International Journal of Robotics Research*, vol. 35, no. 13, 2016.
- [6] A. Carron, E. Arcari, M. Wermelinger, L. Hewing, M. Hutter, and M. N. Zeilinger, "Data-Driven Model Predictive Control for Trajectory Tracking With a Robotic Arm," *IEEE Robotics and Automation Letters*, vol. 4, no. 4, 2019.
- [7] B. Zarrouki, J. Nunes, and J. Betz, "R²NMPC: A Real-Time Reduced Robustified Nonlinear Model Predictive Control with Ellipsoidal Uncertainty Sets for Autonomous Vehicle Motion Control," *IFAC-PapersOnLine*, vol. 58, no. 18, 2024.
- [8] A. Lahr, A. Zanelli, A. Carron, and M. N. Zeilinger, "Zero-order optimization for Gaussian process-based model predictive control," *European Journal of Control*, vol. 74, 2023.
- [9] X. Feng, S. D. Cairano, and R. Quirynen, "Inexact Adjoint-based SQP Algorithm for Real-Time Stochastic Nonlinear MPC," *IFAC-PapersOnLine*, vol. 53, no. 2, 2020.
- [10] A. Zanelli, J. Frey, F. Messerer, and M. Diehl, "Zero-Order Robust Nonlinear Model Predictive Control with Ellipsoidal Uncertainty Sets," *IFAC-PapersOnLine*, vol. 54, no. 6, 2021.
- [11] Y. Gao, F. Messerer, J. Frey, N. van Duijkeren, and M. Diehl, "Collision-free Motion Planning for Mobile Robots by Zero-order Robust Optimization-based MPC," in *2023 European Control Conference (ECC)*, 2023.
- [12] S. Vaskov, R. Quirynen, M. Menner, and K. Berntorp, "Friction-Adaptive Stochastic Predictive Control for Trajectory Tracking of Autonomous Vehicles," in *2022 American Control Conference (ACC)*, 2022.
- [13] P. Polcz, T. Péni, and R. Tóth, "Efficient implementation of Gaussian process-based predictive control by quadratic programming," *IET Control Theory & Applications*, vol. 17, no. 8, 2023.
- [14] J. Gardner, G. Pleiss, K. Q. Weinberger, D. Bindel, and A. G. Wilson, "GPYtorch: Blackbox Matrix-Matrix Gaussian Process Inference with GPU Acceleration," in *Advances in Neural Information Processing Systems*, vol. 31. Curran Associates, Inc., 2018.
- [15] J. A. E. Andersson, J. Gillis, G. Horn, J. B. Rawlings, and M. Diehl, "CasADi: A software framework for nonlinear optimization and optimal control," *Math. Prog. Comp.*, vol. 11, no. 1, 2019.
- [16] R. Verschueren, G. Frison, D. Kouzoupis, J. Frey, N. van Duijkeren, A. Zanelli, B. Novoselnik, T. Albin, R. Quirynen, and M. Diehl, "Acados—a modular open-source framework for fast embedded optimal control," *Math. Prog. Comp.*, vol. 14, no. 1, 2022.
- [17] J. Pohlodek, B. Morabito, C. Schlauch, P. Zomete, and R. Findeisen, "Flexible development and evaluation of machine-learning-supported optimal control and estimation methods via HILO-MPC," *International Journal of Robust and Nonlinear Control*, vol. n/a, no. n/a, 2024.
- [18] E. Picotti, A. D. Libera, R. Carli, and M. Bruschetta, "LbMATMPC: An open-source toolbox for Gaussian Process modeling within Learning-based Nonlinear Model Predictive Control," in *2022 European Control Conference (ECC)*, 2022.
- [19] Z. Yuan, A. W. Hall, S. Zhou, L. Brunke, M. Greeff, J. Panerati, and A. P. Schoellig, "Safe-Control-Gym: A Unified Benchmark Suite for Safe Learning-Based Control and Reinforcement Learning in Robotics," *IEEE Robotics and Automation Letters*, vol. 7, no. 4, 2022.
- [20] F. Fiedler, B. Karg, L. Lüken, D. Brandner, M. Heinlein, F. Brabender, and S. Lucia, "Do-mpc: Towards FAIR nonlinear and robust model predictive control," *Control Engineering Practice*, vol. 140, 2023.
- [21] T. Salzmann, J. Arrizabalaga, J. Andersson, M. Pavone, and M. Ryll, "Learning for CasADi: Data-driven Models in Numerical Optimization," in *Proceedings of the 6th Annual Learning for Dynamics & Control Conference*. PMLR, 2024.
- [22] J. Frey, Y. Gao, F. Messerer, A. Lahr, M. N. Zeilinger, and M. Diehl, "Efficient Zero-Order Robust Optimization for Real-Time Model Predictive Control with acados," 2023.
- [23] A. Carron, S. Bodmer, L. Vogel, R. Zurbrügg, D. Helm, R. Rickenbach, S. Muntwiler, J. Sieber, and M. N. Zeilinger, "Chronos and CRS: Design of a miniature car-like robot and a software framework for single and multi-agent robotics and control," in *2023 IEEE International Conference on Robotics and Automation (ICRA)*, 2023.
- [24] J. Frey, J. D. Schutter, and M. Diehl, "Fast integrators with sensitivity propagation for use in CasADi," in *2023 European Control Conference (ECC)*, 2023.
- [25] M. Diehl, H. G. Bock, and J. P. Schlöder, "A Real-Time Iteration Scheme for Nonlinear Optimization in Optimal Feedback Control," *SIAM J. Control Optim.*, vol. 43, no. 5, 2005.
- [26] H. G. Bock, M. Diehl, E. Kostina, and J. P. Schlöder, "1. Constrained Optimal Feedback Control of Systems Governed by Large Differential Algebraic Equations," in *Real-Time PDE-Constrained Optimization*. Society for Industrial and Applied Mathematics, 2007.
- [27] L. Numerow, A. Zanelli, A. Carron, and M. N. Zeilinger, "Inherently Robust Suboptimal MPC for Autonomous Racing With Anytime Feasible SQP," *IEEE Robotics and Automation Letters*, vol. 9, no. 7, 2024.
- [28] T. Salzmann, E. Kaufmann, J. Arrizabalaga, M. Pavone, D. Scaramuzza, and M. Ryll, "Real-Time Neural MPC: Deep Learning Model Predictive Control for Quadrotors and Agile Robotic Platforms," *IEEE Robotics and Automation Letters*, vol. 8, no. 4, 2023.
- [29] G. Frison, D. Kouzoupis, T. Sartor, A. Zanelli, and M. Diehl, "BLAS-FEO: Basic Linear Algebra Subroutines for Embedded Optimization," *ACM Trans. Math. Softw.*, vol. 44, no. 4, 2018.
- [30] A. Liniger, A. Domahidi, and M. Morari, "Optimization-based autonomous racing of 1:43 scale RC cars," *Optimal Control Applications and Methods*, vol. 36, no. 5, 2015.
- [31] C. E. Rasmussen and C. K. I. Williams, *Gaussian Processes for Machine Learning*, ser. Adaptive Computation and Machine Learning. Cambridge, Massachusetts: MIT Press, 2006.
- [32] M. A. Osborne, "Bayesian Gaussian processes for sequential prediction, optimisation and quadrature," Ph.D. dissertation, Oxford University, UK / Oxford University, UK, 2010.